Electronic supplementary information:

Pervaporation-Assisted *In Situ* Formation of Nanoporous Microchannels with Various Structural and Material Properties

Sangjin Seo,[a] Juyeol Bae,[a] Hwisu Jeon,[a] Sungyoon Lee,[a] and Taesung Kim[a,*]

[a]Department of Mechanical Engineering, Ulsan National Institute of Science and Technology (UNIST), 50 UNIST-gil, Ulsan 44919, Republic of Korea

CORRESPONDENCE:

Taesung Kim
Department of Mechanical Engineering
Ulsan National Institute of Science and Technology (UNIST)
50 UNIST gil, Ulsan 44919, Republic of Korea
E mail: tskim@unist.ac.kr
Tel: +82 52 217 2313
Fax: +82 52 217 2449

Supplementary Notes

Note S1: Molecular transport inside the bridge channel with PIF

Even though Péclet number, $\mathrm{Pe}_{\mathrm{FITC}} = v_{x,\mathrm{avg}}(-L)L / D_{\mathrm{FITC}} = 8.42$, calculated using PIF of the bridge channel (regardless of PAM) is much lower than the criterion (Pe = 26.1) suggested in our previous research[1], the fluorescent molecules continuously concentrated at the center of the bridge channel. In order to elucidate this conflict, we investigated the advantages of PAM for molecular concentration. Two effects were considered here: (i) The PAM increases the effective flow velocity by reducing the volume of the bridge channel while the pervaporation rate through the gas-permeable film remains constant. Thus, the continuity equation along the uniform-rectangular-shaped bridge channel with a constant pervaporation flux can be written as follows:

$$v_{x,\mathrm{avg}}(x)A_{\mathrm{c}} - v_{x,\mathrm{avg}}(x+dx)A_{\mathrm{c}} = \frac{J}{\rho} w dx \tag{1}$$

$$A_{\mathrm{c}} = \frac{\delta V}{dx} = (1-\phi)wh \tag{2}$$

where A_{c} is the averaged cross-sectional area in the consideration of the volume reduction due to the PAM, δV is the infinitesimal of vacant volume and ϕ is the packing fraction of the PAM. Then,

$$\overline{v}_{x,\mathrm{avg}}(x) = -\frac{Jx}{\rho \overline{h}} \tag{3}$$

where $\overline{h} = (1-\phi)h$ is the effective height, which is a determinative parameter to the PIF velocity along the uniform-rectangular-shaped bridge channel filled with PAM. As the packing fraction of the PAM increases, the PIF velocity increases proportionally with the decreaing volume. (ii) The molecular diffusion is slower in the bridge channel filled with the PAM than that in an empty bridge channel. The effective diffusion coefficient of the solute in the solvent in the porous structure is[2]:

$$D_{i,\mathrm{eff}} = \frac{D_i}{\tau} \tag{4}$$

where τ is the tortuosity is equivalent with a fractional increase of diffusion path length[3].

Furthermore, for the PAM made of monodisperse spherical particles without particle overlapping, the tortuosity is related to the porosity (ε), which is also related to the packing fraction as follows[4]:

$$\tau = \frac{3-\varepsilon}{2} = \frac{2+\phi}{2} \tag{5}$$

The effective Péclet number and the determinative parameter for transport control of small molecules using PIF can be re-written as follows:

$$\overline{\mathrm{Pe}_i} = \frac{\overline{v}_{x,\mathrm{avg}}(-L)L}{D_{\mathrm{i,eff}}} = \overline{\phi}\,\frac{JL^2}{\rho h D_i} \tag{6}$$

where

$$\overline{\phi} = \frac{2+\phi}{2-2\phi} \tag{7}$$

Note S2: Geometric modification for faster inlet flow velocity

Fig. S5 shows a simple modification of the microchannel geometry that can provide more choice of target molecule and flexibility in device design. Fig. S5a describes a channel design with modified inlet width, w_{in}, while the pervaporation area ($w \times L$ for a half side) is fixed. An additional 30-μm-long inlet was added at each end and yellowish triangular areas were removed by the area increased due to the additional inlet. With a variable width, w(x) cross-sectional area can be re-written as:

$$A_{\mathrm{c},w}(x) = \frac{\delta V}{dx} = w(x)h \tag{8}$$

Then, with $A_{\mathrm{c},w}(x)$, instead of constant A_{c}, Equation (1) is simplified as a non-homogeneous linear ordinary differential equation:

$$\frac{d(v_{x,\mathrm{avg}}(x))}{dx} + \frac{1}{w(x)}\frac{d(w(x))}{dx}v_{x,\mathrm{avg}}(x) = \frac{J}{\rho\,\mathrm{h}} \tag{9}$$

Using the general solution,

$$v_{x,\mathrm{avg}}(x) = \frac{J}{\rho h}\frac{\int w(x)dx}{w(x)} \tag{10}$$

The analytical solution is plotted in Fig. S5b as solid lines with four different sizes of the inlet. The 3-D numerical simulation results are displayed as dots in the shape to show that 1-D analytical solutions and 3-D numerical solutions agree well with each other. The width reduces from the center to the region before the channel (e.g., in the case of w_{in} = 10 μm, from x = 0 μm to x = −380 μm), the average velocity remains constant regardless of the inlet size. In the narrowing region (e.g., for w_{in} = 10 μm from x = −380 μm to x = −400 μm), the average velocity increased significantly and in the inlet region (e.g., in the case of w_{in} = 10 μm, from x = − 400 μm to x = −430 μm), velocity increased slightly further with the same slope of the first region. From the viewpoint of constant pervaporative mass flow-rate through the entire bridge channel, the average inlet velocity is inversely proportional to the inlet size, as shown in Fig. S5b. Using the PTV analysis in Fig. 2, the velocity at the inlet was measured as shown in Fig. S5c. The theoretical prediction by $v_{avg,x} = \alpha/w_{in}$ is plotted (blue dashed line) using the point of w_{in} = 40 μm as a reference to calculate the coefficient, α. The fitting curve (red solid line) of data shows inversely proportional relation, consistent with the theoretical prediction. We verified that the inlet flow velocity can be increased using a simple modification of the bridge channel geometry. With a faster flow velocity at the inlet, it is expected to be able to control the transport of molecules which have faster diffusion behavior than FITC. Moreover, the length of the bridge channel, which is a critical parameter ($Pe_i \sim L^2$) for maintaining the device performance, can be reduced. However, as the bridge channel becomes shorter, the diffusion time ($t_D = L^2/2D$) also decreases, which may require further parametric studies and experimental validation.

Supplementary Figures

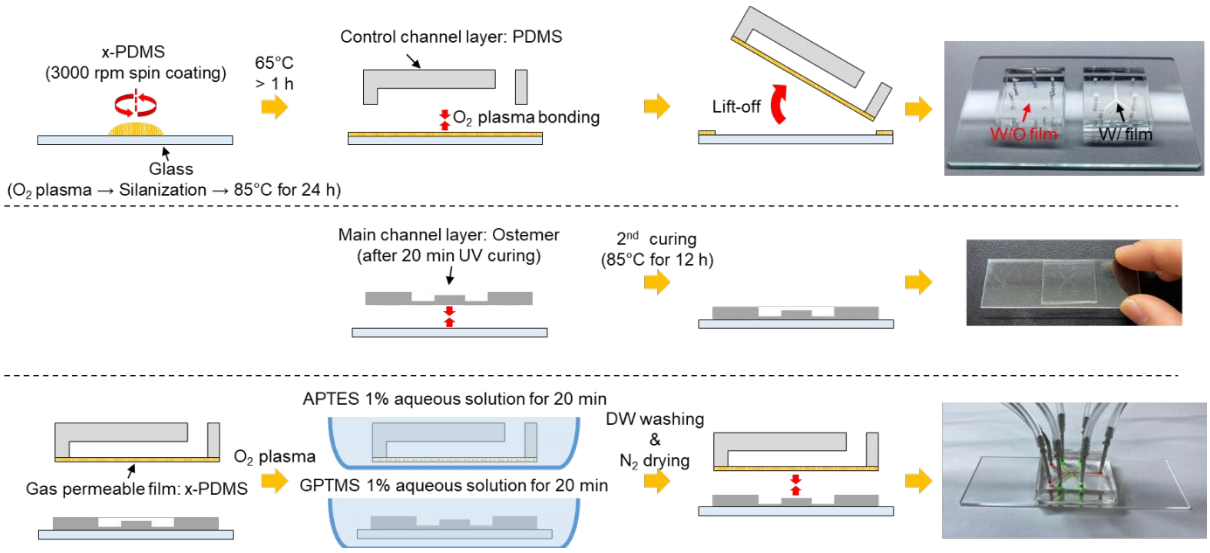

Fig. S1. Fabrication process of PAMs and PAM-integrated micro-/nanofluidic devices. **(Top row)** The control-channel layer is fabricated using a silanized (trichloro(1H,1H,2H,2H-perfluorooctyl)silane) SU-8 mold and PDMS via soft-lithography. The control-channel layer is cured using an oven at 65 °C for 3 h. The gas-permeable film is fabricated by spin-coating x-PDMS on a silanized (chloromethylsilane) glass substrate. Using a surface profiler, the film thickness was measured to be 12.4 μm. The control-channel layer and film are bonded using O_2 plasma treatment. At least 10 min after bonding, the edges of the bonded area of the film was cut and peeled off, resulting in easy peeling-off of the control-channel layer, while the bottom is covered by the x-PDMS film. **(Middle row)** The main-channel layer is fabricated in a similar manner as the control-channel layer, but Ostemer Flex 324 is used instead of PDMS. This layer is initially cured using 312 nm UV for 20 min and then thermally cured at 85 °C for 12 h for bonding to the glass substrates. **(Bottom row)** The two layers are bonded together with their processed surfaces facing each other. After O_2 plasma treatment on both the devices, the film-bonded control channel device is immersed in the aqueous solution of APTES (1% v/v) and the main channel device on the glass substrate is immersed in the (1% v/v) aqueous solution of GPTMS for 20 min each. After the devices are washed with DW and dried using with N_2, the devices are covalently bonded, completing the fabrication process of the microfluidic device.

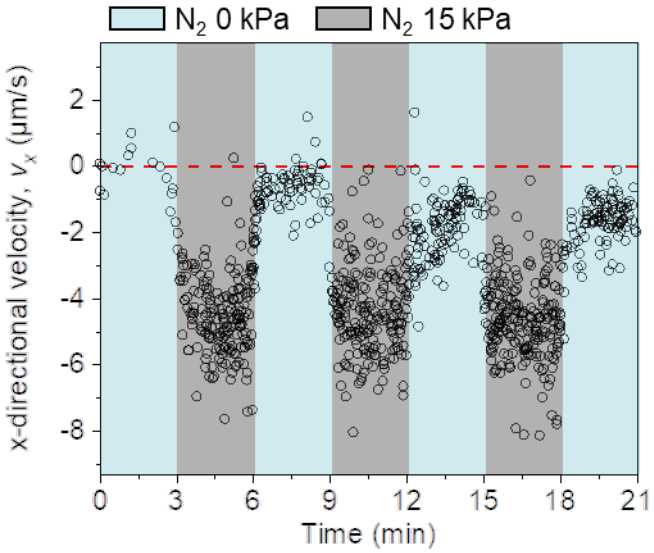

Fig. S2. Particle velocities inside the ROI measured by PTV under repeatedly switching pervaporation conditions. The pervaporation condition was switched repetitively at 3 min intervals using dried N_2 gas without DW injection to the control channel. The particle velocities showed relatively slow responses compared to the switching conditions using both dried N_2 gas and DW. With passage of time, both the response time and the repeatability deteriorate, implying that the combination of N_2 gas and DW yields better performance .

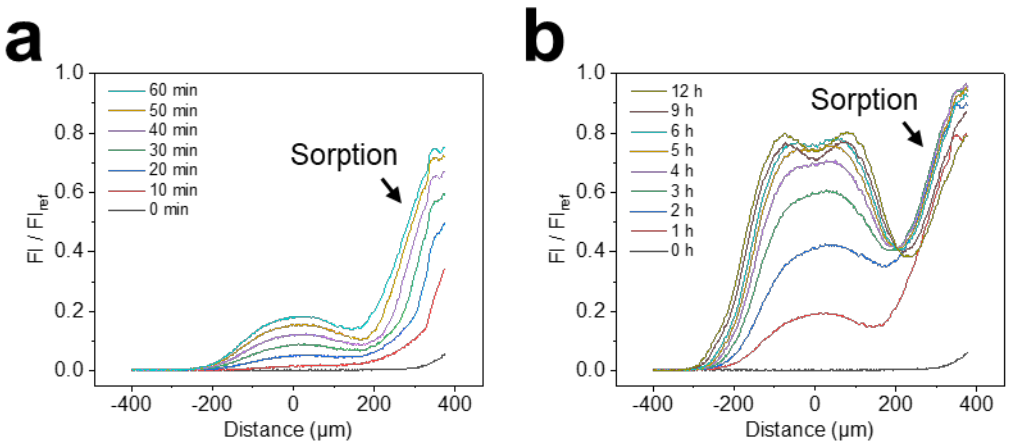

Fig. S3. Normalized fluorescence intensity of FITC molecule concentration over time. a) For the first 1 h. b) For the entire 24 h period.

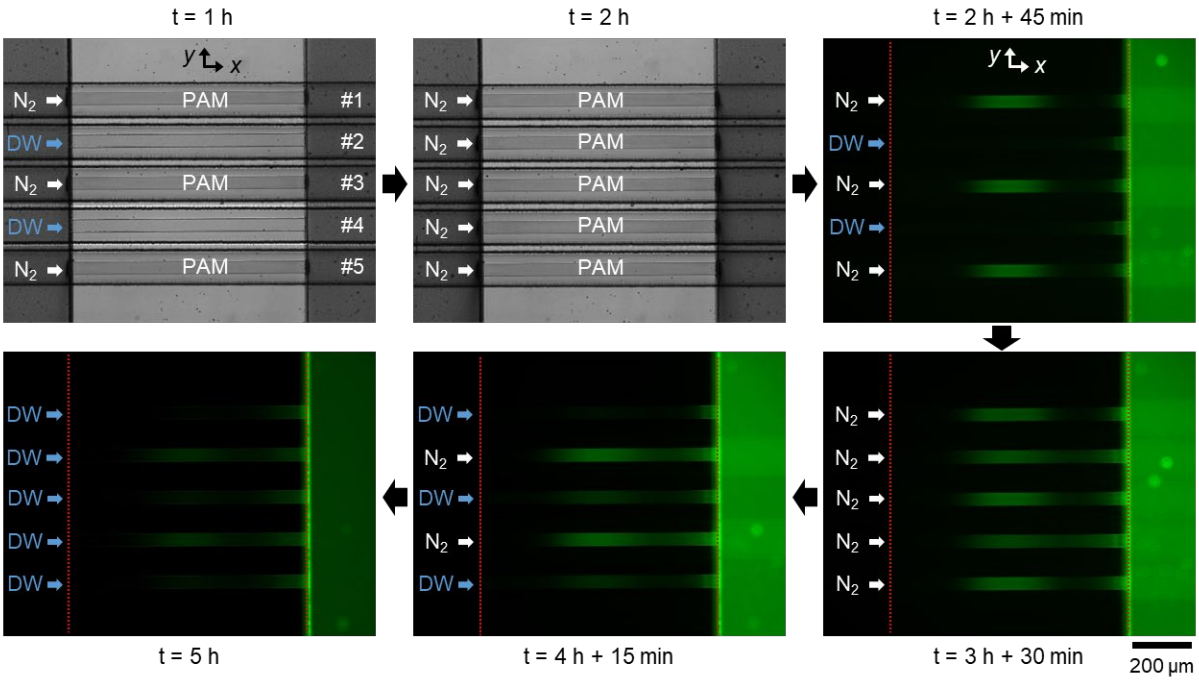

Fig. S4. Individual and selective controllability of multiple PAM-integrated microchannels. The top control-channel layer was designed to have a selective addressability to the designated bridge channels in the bottom main channels through the thin gas-permeable film. This further makes it possible to individually control the PIF in the bride channels. First, N_2 gas was injected into odd-numbered control channels, enabling the selective formation of PAMs (t = 1 h). Second, the PAMs were formed in the remaining bridge channels in a similar manner via individual control (t = 2 h). Third, FITC solution was introduced at the right main channel and then the odd-numbered and even-numbered control channels were separately operated, manipulating the molecular transport in the bridge channels in a controlled manner, as shown in the Fig. (t = 2.75 h). N_2 gas injection induced PIFs, which in turn concentrated FITC molecules at the center of the odd-numbered bridge channels. On the other hand, DW injection prevented FITC molecules from concentrating because no PIF was generated. Fourth, N_2 gas was injected in all the control channels, resulting in the concentration of FITC molecules at the center of the bridge channels (t = 3.5 h). Fifth, the pervaporation conditions were changed at the control channels, and the conditions were the converse of those in the third step (t = 4.25 h). The odd-numbered bridge channels lost fluorescence signals while the even-numbered ones retained them. This can be attributed to the PIF-based concentration and PIF-

free diffusion. This result was further validated by introducing DW into all the control channels, resulting in low fluorescence intensities (t = 5 h).

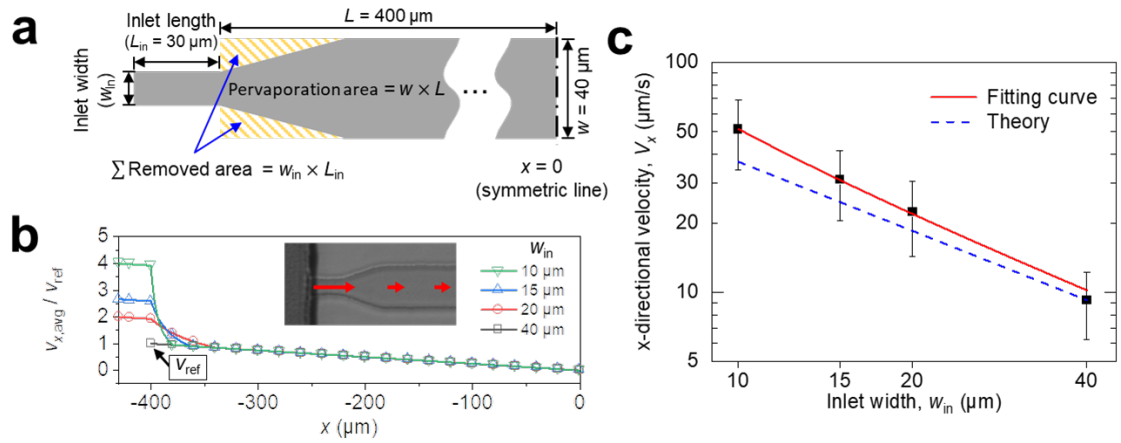

Fig. S5. Geometric modification of the bridge channel increases the inlet velocity. a) Schematic illustration showing the modified design of the entrance of the bridge channel. According to the fluid continuity, the flow velocity at the entrance becomes faster by narrowing the inlet as shown in the Fig.. In addition, the net area of the original bridge channel was intentionally reduced, which is indicated with yellow hatched lines. The reduced area is the same as the newly added inlet, which makes it possible to maintain the constant pervaporation area. **b)** Theoretical prediction (solid lines) and numerical simulation results (shaped dot) for different widths of the inlets; all of them have the same pervaporation area. Both the experimental and simulation results match well, exhibiting the steep increase of the flow velocity only at the inlet, while the same velocities are maintained after the new inlet along the bridge channel. The inset optical image shows a modified inlet (15 μm) of the bridge channel with red arrows indicating the flow velocity. **c)** The flow velocities near the inlet of the bridge channel were obtained using PTV. The blue dashed line shows the curve fitting result based on the reciprocal relationship between the inlet width and the flow velocity. The experimental result also shows a similar reciprocal relationship, consistent with the curve-fitting result.

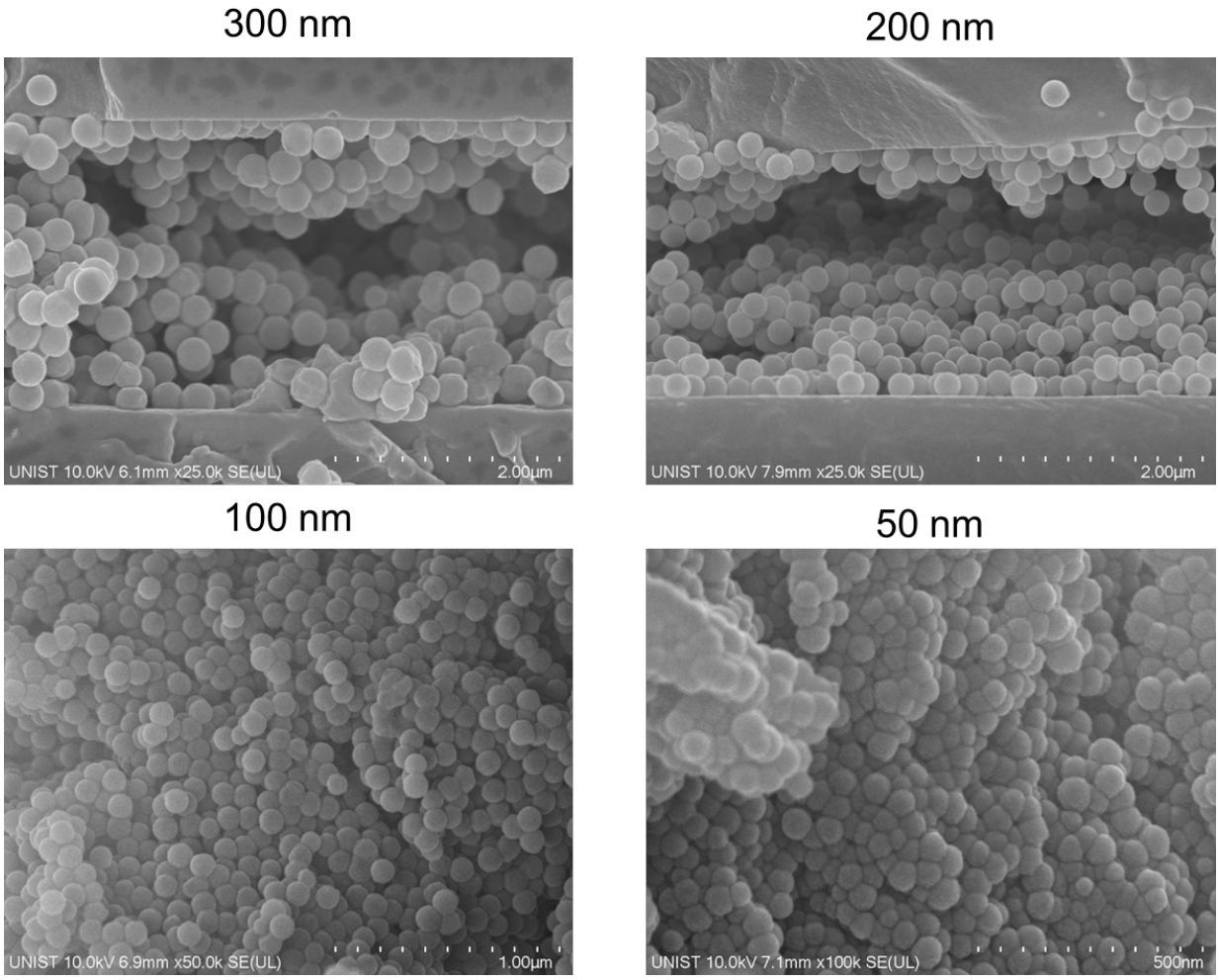

Fig. S6. SEM images of PAMs in the bridge channel containing several different-sized PS particles. PAMs show random close packed structures.

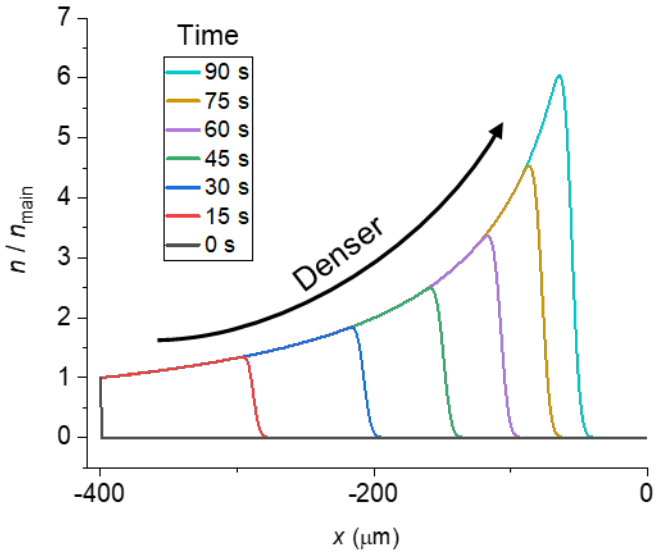

Fig. S7. Numerical simulation result of the number density of particles using the diffusion–advection equation. The number density of particles along the bridge channel (i.e., from x = –400 μm to x = 0) was normalized with the mean number density in the main channel. The PIF velocities gradually decrease as the particles flow toward the center of the bridge channel, thus attaining the maximum number density near the center. Because the number density increases along the bridge channel, 500-nm particles, the diameter of which is comparable to the height of the bridge channel, aggregate before they reach the center of the bridge channel. The diffusion coefficients of the particles were estimated by using Stokes–Einstein equation.

Supplementary Movies

Movie S1: Assembly of 200-nm PS particles in a bridge channel.

Movie S2: Concentration of FITC molecules in the PAM-integrated microchannel.

Movie S3: Convection of fluorescent particles in the bare bridge channel when the pervaporation conditions of the control channel are repeatedly switched.

Movie S4: Convection of fluorescent particles at the inlet of the modified bridge channel (w_{in} = 10 μm).

Movie S5: Concentration of sulforhodamine B sodium molecules in a PAM array having two different surface modifications.

Movie S6: Release of concentrated sulforhodamine B sodium molecules in a PAM array made of two different, surface-modified particles.

Movie S7: Wetting a PAM array made of hydrophobic and hydrophilic particles with mineral oil.

Movie S8: Aqueous FITC solution obtained by replacing the mineral oil filling the hydrophilic PAM (and not the hydrophobic PAM).

References

[1] S. Seo, D. Ha, T. Kim, Nat. Commun. 2021, 12, 1336.

[2] A. M. Berezhkovskii, V. Y. Zitserman, S. Y. Shvartsman, J. Chem. Phys. 2003, 119, 6991–6993.

[3] W. M. Saltzman, R. Langer, Biophys. J. 1989, 55, 163–171.

[4] S. Bellini, G. Azzato, M. Grandinetti, V. Stellato, G. De Marco, Y. Sun, A. Caravella, Appl. Sci. 2018, 8, 573.